ChemComm

Accepted Manuscript

This article can be cited before page numbers have been issued, to do this please use: Y. Song, T. Xu, L. Xu and X. Zhang, *Chem. Commun.*, 2019, DOI: 10.1039/C8CC09586H.

This is an Accepted Manuscript, which has been through the Royal Society of Chemistry peer review process and has been accepted for publication.

Accepted Manuscripts are published online shortly after acceptance, before technical editing, formatting and proof reading. Using this free service, authors can make their results available to the community, in citable form, before we publish the edited article. We will replace this Accepted Manuscript with the edited and formatted Advance Article as soon as it is available.

You can find more information about Accepted Manuscripts in the author guidelines.

Please note that technical editing may introduce minor changes to the text and/or graphics, which may alter content. The journal's standard Terms & Conditions and the ethical guidelines, outlined in our author and reviewer resource centre, still apply. In no event shall the Royal Society of Chemistry be held responsible for any errors or omissions in this Accepted Manuscript or any consequences arising from the use of any information it contains.

ROYAL SOCIETY OF CHEMISTRY

rsc.li/chemcomm

View Article Online
DOI: 10.1039/C8CC09586H

Journal Name

COMMUNICATION

Nanodendritic Gold/Graphene-Based Biosensor for Tri-Mode miRNA Sensing

Yongchao Song, Tailin Xu*, Li-Ping Xu*, Xueji Zhang*

Received 00th January 20xx,
Accepted 00th January 20xx

DOI: 10.1039/x0xx00000x

www.rsc.org/

Nanodendritic gold/graphene-based biosensor that can perform fluorescence, SERS and electrochemistry tri-mode miRNA detection in single microdroplet has been presented. Such biosensor successfully performed the tri-mode quantitative trace miRNA-375 detection, which enormously reduces the false positive causing by interference and ambiguous signals, and provides significant implications for precisely physiological and pathological diagnosis.

The chemical and biological sensors with various signal output approaches (SERS, fluorescence, electrochemistry, and colorimetric et al.) have received considerable attentions for early diagnosis and real-time monitoring.[1-4] Although each approach has its own advantages, no single technique is capable of giving complete information due to its intrinsic drawbacks in terms of sensitivity, multiplexing capability and response time. Superior to traditional single-signal platforms, multiple output signals provide a booming option to eliminate the interference and ensure the accuracy of detection by the multiple sets of data coupling and validating mutually.[5-9] For example, the combination of fluorescence and colorimetry has achieved highly sensitive detection of aptamer,[10] arginine,[11, 12] and thrombin.[13] The colorimetrical and electrochemical dual-signal sensors have achieved precise detection of food bacteria,[14] metals,[15]and drugs.[16] The fluorescence-SERS dual-signal platform has accomplished high throughput molecular recognition.[17, 18] However, most multiple platforms are confined in dual-mode sensing, and there are still much room to fabricate the multiplexed biochips and achieve 'all in one' for multimodal and multifunctional sensing applications to meet high-demand clinical sensing.

The extremely wettable surfaces have attracted considerable attention in chemistry, biology, medicine, and diagnostics.[19-21] With the miniaturization and parallelization of micropatterns, such surfaces have successfully achieved complex geometries microdroplets array for nanoparticle assembly, polymer deposition and high-throughput cell screening.[22-29] Recently, several wettable pattern based sensing biochips have been fabricated, and achieved high-sensitive analyte identification by integrating with SERS,[30-36] electrochemical,[37, 38] fluorescent or other sensing technologies.[39-44] Such open-channel operating mode platform provides potential opportunity to integrate multi-signal outputting approaches, and achieves multimodal and multifunctional sensing for biological and chemical application.

Here we fabricated a unique multifunctional nanoplatform based on the graphene/nanodendritic gold substrate for tri-mode miRNA biosensing, which has been achieved by intergrating fluorescence, SERS and electrochemical approaches as demonstrated in **Figure 1**. Based on the nanodendritic structure of gold electrode, the electrochemical and Raman signals can be improved due to the high electron transmission efficiency and the enhanced surface Ramon scattering. Concurrently, the existence of graphene can realize fluorescent response due to the different absorption behavior between single and double nucleic acid strand. Compared with traditional sensors, the tri-mode sensing platform can

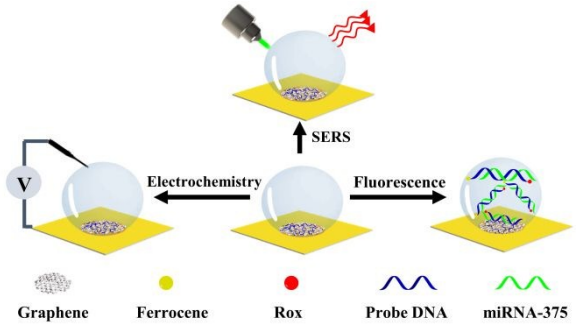

Figure 1. Schematic illustration of nanodendritic gold/graphene-based droplet biosensor for tri-mode (Fluorescent, electrochemical and SERS) miRNA sensing.

Research Center for Bioengineering and Sensing Technology, School of Chemistry and Biological Engineering, University of Science and Technology Beijing, Beijing 100083, P. R. China.
**xutailin@ustb.edu.cn; xuliping@ustb.edu.cn; zhangxueji@ustb.edu.cn*
Electronic Supplementary Information (ESI) available: [details of any supplementary information available should be included here]. See DOI: 10.1039/x0xx00000x

enormously distinguish the false positive detection causing by interference and ambiguous signals by the multiple sets of data coupling, which provides the great potential in multimodal and multifunctional sensing for precise disease diagnosis.

The multiplexed nanodendritic gold/graphene-based biochip is fabricated as shown in **SI Figure 1**. In brief, we sputtered a layer of titanium and gold on the conductive side of ITO for enhancing the adhesion of nanodendritic gold. Then, the nanodendritic gold was electrodeposited on the ITO/Ti/Au electrode at −1.8 V for 1800 s in an electrolyte composed of sulfuric acid (0.5 M) and $HAuCl_4$ (1 mg/mL). Further, the nanodendritic gold substrate was immersed in the dodecanethiol solution (10 vol. % in ethanol) for 24 h for hydrophobic modification. After that, the oxygen plasma was used to decompose partial dodecanethiol to form superhydrophilic region with the diameter of 1 mm through a home-made photomask. Such superhydrophilic region can immobilize the microdroplets up to 30 ul. Thus, the superwettable nanodendritic gold biochip was fabricated as shown in **SI Figure 1a**. Next, the dispersed graphene sheets (0.5 mg/mL) suspension was prepared, and then transferred to the superhydrophilic nanodendritic gold microwell.[45] As the moisture evaporation, the graphene was precisely deposited in the superhydrophilic microwell. Thus, nanodendritic gold/graphene-based biochip was successfully fabricated as shown in **SI Figure 1b**.

The morphology of such nanodendritic gold/graphene biochip was demonstrated in **Figure 2b**. The electrodeposited gold has highly branched three-dimensional structures with large surface area and high density of sharp tips as shown in **Figure 2b** left. After the graphene deposition, several microsheet can be observed in **Figure 2b** right, and C element (red) in EDX elemental map in **SI Figure 2a** demonstrated the successfully deposition of graphene on the nanodendritic gold. As shown in **SI Figure 2b,** the clear boundary of nanodendritic gold/graphene and gold nanodendrites can be found in the designated region. The stability of substrate is essential for carrying out accurate and reliable detection. The graphene in superhydrophilic nanodendritic gold microwell is fairly stable, presenting no shedding under rinsing with water and ethanol for a few minutes respectively (**SI Figure 3 and SI Video 1**).

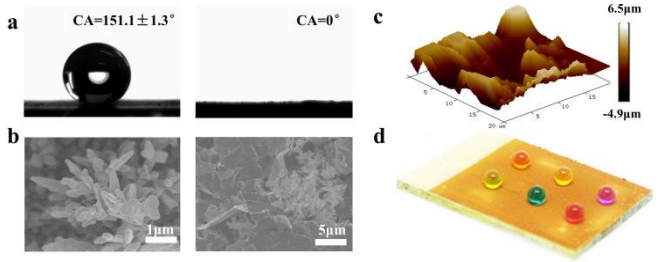

Figure 2. a) Water contact angles of dodecylmercaptan modified nanodendritic gold substrate (left) and after O2 plasma etching (right). b) SEM images of the nanodendritic gold (left) and nanodendritic gold/graphene substrate (right). c) AFM image of nanodendritic gold/graphene substrate. d) Dye-labeled water microdroplets on such biosensor.

The ability of microdroplet manipulation depends on the wettability of substrate. For the hydrophilic substrates of ITO and bare gold (**SI Figure 4a, 4b**), the microdroplets tend to spread over the larger area and form irregular shapes. While on the nanodendritic gold substrate, the microdroplet is flattened completely with contact angle of 0°, revealing its superhydrophilicity. In comparison, after hydrophobic modification, nanodendritic gold substrate demonstrated the extreme water repellency with the contact angle of 151.1±1.3° due to the low surface energy of dodecanethiol (**Figure 2a, left**), revealing its superhydrophobicity. After 2 min O_2 plasma irradiation, the contact angle restored back to 0° (**Figure 2a, right**). Notably, the high roughness of the substrate (1.76 μm) (**Figure 2c**) and the presence of carbonyl and carboxyl groups of the graphene in superhydrophilic microwell is helpful for superhydrophilicity (**SI Figure 4c**).[46] Thus the biochip exhibits the outstanding performance for anchoring microdroplets in nanodendritic gold/graphene microwells (**Figure 2d**).

Different substrates including bare ITO, bare gold, nanodendritic gold and nanodendritic gold/graphene substrates are compared to perform the fluorescent, SERS and electrochemical detection. For fluorescent performance, the ITO, bare gold and nanodendritic gold substrates have insignificant ssDNA adsorption, and considerable fluorescence peaks were found in supernatant as demonstrated **SI Figure 5b,** while nanodendritic gold/graphene substrate showed excellent adsorption performance with almost no fluorescence signal in supernatant. For the SERS performance, the ITO substrate had no distinguishable Raman peaks, and the bare gold substrate had almost no Raman enhanced effects. In contrast, the nanodendritic gold demonstrated the spectacular SERS signals, and the presence of graphene weakened the signal while still maintained relatively Raman enhancement effects as shown in **SI Figure 5c**. For electrochemical measurement, the introduced graphene has no obviously influence on the electrochemical

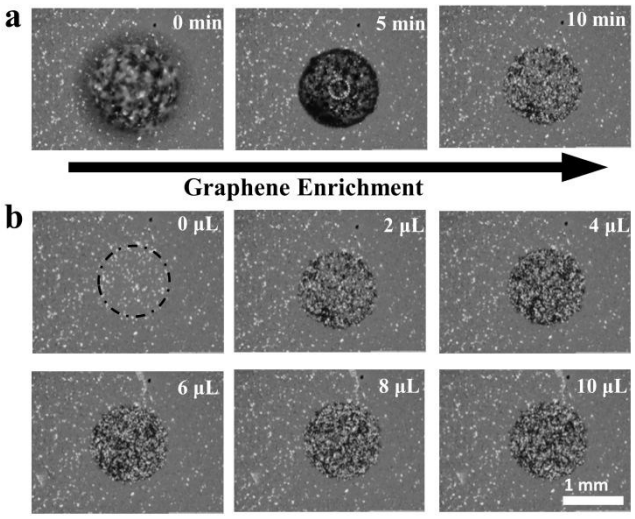

Figure 3. a) Processes of graphene assembly in the superhydrophilic microwell. b) Optical microscope images of graphene deposited in the superhydrophilic microwell as increasing volumes of graphene aqueous solution (0, 2, 4, 6, 8 and 10 μL, 0.5 mg/mL).

View Article Online
DOI: 10.1039/C8CC09586H

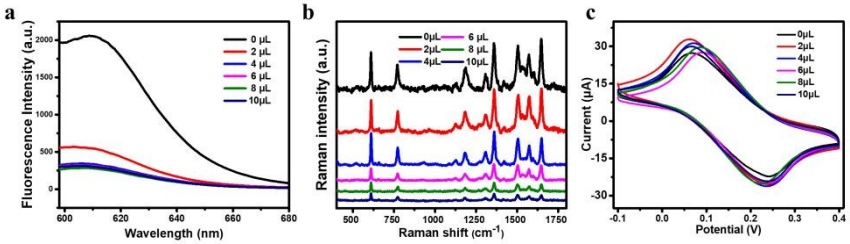

Figure 4. The effect of graphene amount (0, 2, 4, 6, 8 and 10 μL, 0.5 mg/mL) on the a) fluorescent (10 μM ROX-modified DNA supernatant), b) SERS (10 μM R6G-containing droplets) and c) electrochemical (5 mM potassium ferricyanide/ferrocyanide and 100 mM NaCl in PBS buffer) sensing.

signal comparing with the nanodendritic gold, so both nanodendritic gold and nanodendritic gold/graphene are suitable for highly sensitive electrochemical sensing as shown in **SI Figure 5d**. However, the bare Au and ITO electrode only had weak electrochemical signal. Based on above discussion, the nanodendritic gold/graphene substrates show excellent fluorescent, SERS and electrochemical response performance.

The amount of graphene in superhydrophilic microwells was also optimized to get the nanodendritic gold/graphene-based tri-mode biochip for getting better fluorescent, SERS and electrochemical signals. For minimizing the deviations caused by different nanodendritic gold substrate, different volumes suspension (0, 2, 4, 6, 8 and 10 μL, 0.5 mg/mL) was carefully dropwise added in six microwells on the same biochip. The graphene suspension can be anchored at the microwell and the graphene can be well in situ deposited after water evaporation as shown in **Figure 3a**. The distribution of graphene was relatively homogeneous in microwells and covered more area of nanodendritic gold with the increasing the amount of graphene as demonstrated in **Figure 3b** and **SI Figure 6**. For the fluorescence detection, no obvious DNA adsorption occurred on the substrate without graphene (0 μL) according to the considerable fluorescence peak in supernatant. In comparison, the decrease fluorescence intensity in supernatant (2 μL, 0.5 mg/mL) indicates that part of DNA was absorbed by the graphene in the microwell. Subsequently, the contained microwells containing more graphene (4, 6, 8 and 10 μL, 0.5 mg/mL) further decreased the fluorescence signal and maintained to negligible intensity, revealing the saturation of target DNA adsorption as shown in **Figure 4a**. For SERS sensing, the signal is strongest in the absence of graphene, and the Raman signal decreases gradually with the increase of the amount of graphene in the superhydrophilic microwells (**Figure 4b**). The electrochemical results show that curves are just subtly difference with the increasing amount of graphene as shown in **Figure 4c**. To balance optimal signals outputting of fluorescent and SERS, 4 μL graphene (0.5 mg/mL) was chosen to fabricate the optimal nanodendritic gold/graphene-based biochip for carrying out multimodal miRNA sensing.

The prostate cancer specific biomarker miRNA-375 is chose as target molecule to perform fluorescence, SERS and electrochemical sensing in such nanodendritic gold/graphene-based biochip for evaluating its versatility and feasibility. The Rhodamine X (ROX) and ferrocene modified DNA probe was adsorbed in the microwell due to the strong interaction between graphene and single strand DNA. With the present of miRNA-375, the probe DNA was desorbed to supernatant due to the weak interaction of double-stranded nucleic acid with graphene. The supernatant has significant fluorescence emancipation (**SI Figure 7**), and the substrate containing the remaining probe DNA was interrogated by Raman Spectroscopy and electrochemical respectively (**Figure 5**). For the fluorescent verification, the fluorescence peak intensity increased with the increasing of concentration of miRNA and has a linear relationship with concentration from 10^{-13} to 10^{-9} M, and a correlation coefficient is 0.9934. The detection limit is estimated to be 0.43 pM. For the SERS sensing, the specific Raman signals of ROX at ~1499 and 1644 cm^{-1} were discovered and decreased with the increasing miRNA. The corresponding calibration plot of ~1644 cm^{-1} peak intensity vs miRNA concentration is linear with correlation coefficient of 0.9876. The detection limit is estimated to be 1.13 nM. For the electrochemistry measurement, the electrochemical signal decreased gradually with the increasing of miRNA-375 concentration, and has a good linear with correlation coefficient of 0.9805. The detection limit is estimated to be 0.34 nM. Integrating tri-mode LODs, the biosensor detection range is from 0.43 pM to 1.13 nM under our experimental conditions. Thus such biosensor has exhibited excellent performance for tri-mode quantitative miRNA-375 sensing.

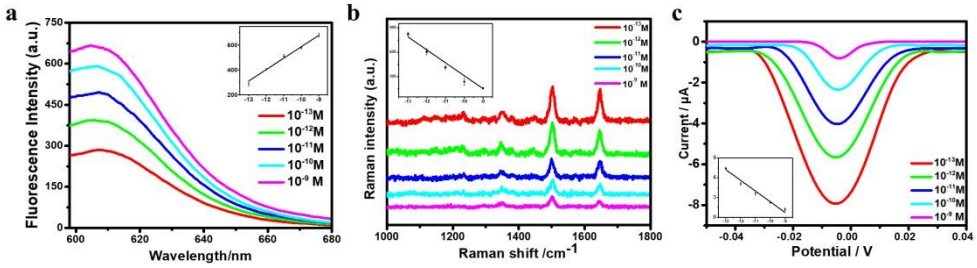

Figure 5. Nanodendritic gold/graphene-based biosensor for tri-mode miRNA detection. a) Fluorescence spectra in the presence of miRNA-375 with concentrations of 10^{-9}, 10^{-10}, 10^{-11}, 10^{-12} and 10^{-13}. b) SERS spectra and c) Differential pulse voltammogram (DPV) in the presence of miRNA-375 with concentrations of 10^{-13}, 10^{-12}, 10^{-11}, 10^{-10}, and 10^{-9} M. Insets show the linear relationship between Fluorescence signal (a) / SERS signal at 1644 cm^{-1} (b) / Electrochemical signal (c) and different concentrations miRNA-375.

In conclusion, we have demonstrated the versatile sensing platform for tri-mode biosensing by integrating fluorescence, SERS and electrochemical approaches with the extremely wettable surfaces. Such tri-mode biosensor is simply prepared via electrochemical deposition, patterning and graphene assembly. Specifically, the superhydrophilic detection spots surrounding by the superhydrophobic background, which is essential for anchoring the microliter droplets. Benefiting from the large surface area and high density hotspots of nanodendritic gold, the microwell can carry out sensitively electrochemical sensing and SERS detection. Meanwhile the introduced graphene with different absorption behavior between single and double nucleic acid strand provides the fluorescent signal response. The tri-mode detection of miRNA-375 has been achieved successfully, which improved the accuracy of noninvasive biomarker sensing by the multiple sets of data coupling, demonstrating potential applications in precisely early diagnosis and real-time monitoring.

We acknowledge funding from National Natural Science Foundation of China (21804007, 21727815, and 21475009), Beijing Natural Science Foundation (2184109, 2182036), Fundamental Research Funds for Central Universities (FRF-TP-17-066A1), and National Postdoctoral Innovative Talents Support Program of China (BX20180036).

Conflicts of interest

There are no conflicts to declare.

Notes and references

1 K. P. Carter, A. M. Young and A. E. Palmer, *Chem. Rev.*, 2014, **114**, 4564-4601.
2 D. G. Rackus, M. H. Shamsi and A. R. Wheeler, *Chem. Soc. Rev.*, 2015, **44**, 5320-5340.
3 S. Zeng, D. Baillargeat, H. P. Ho and K. T. Yong, *Chem. Soc. Rev.*, 2014, **43**, 3426-3452.
4 M. Labib, E. H. Sargent and S. O. Kelley, *Chem. Rev.*, 2016, **116**, 9001-9090.
5 C. Hagleitner, A. Hierlemann, D. Lange, A. Kummer, N. Kerness, O. Brand and H. Baltes, *Nature*, 2001, **414**, 293-296.
6 A. Y. Zhu, F. Yi, J. C. Reed, H. Zhu and E. Cubukcu, *Nano Lett.*, 2014, **14**, 5641-5649.
7 P. Wu, L. N. Miao, H. F. Wang, X. G. Shao and X. P. Yan, *Angew.Chem. Int. Ed.*, 2011, **50**, 8118-8121.
8 Z. Li, J. R. Askim and K. S. Suslick, *Chem. Rev.*, 2018, DOI: 10.1021/acs.chemrev.8b00226.
9 J. S. Choi, Y. W. Jun, S. I. Yeon, H. C. Kim, J. S. Shin and J. Cheon, *J. Am. Chem. Soc.*, 2006, **128**, 15982-15983.
10 C. Y. Hui, M. Liu, Y. Li and J. D. Brennan, *Angew. Chem. Int. Ed.*, 2018, **57**, 4549-4553.
11 T. Liu, N. Li, J. X. Dong, Y. Zhang, Y. Z. Fan, S. M. Lin, H. Q. Luo and N. B. Li, *Biosens. Bioelectron.*, 2017, **87**, 772-778.
12 W. Lu, Y. Gao, Y. Jiao, S. Shuang, C. Li and C. Dong, *Nanoscale*, 2017, **9**, 11545-11552.
13 W. Duan, X. Wang, H. Wang and F. Li, *Talanta*, 2018, **180**, 76-80.
14 J. A. Adkins, K. Boehle, C. Friend, B. Chamberlain, B. Bisha and C. S. Henry, *Anal. Chem.*, 2017, **89**, 3613-3621.
15 P. Rattanarat, W. Dungchai, D. Cate, J. Volckens, O. Chailapakul and C. S. Henry, *Anal. Chem.*, 2014, **86**, 3555-3562.
16 T. G. Silva, W. R. de Araujo, R. A. Munoz, E. M. Richter, M. H. Santana, W. K. Coltro and T. R. Paixao, *Anal. Chem.*, 2016, **88**, 5145-5151.
17 S. Zong, Z. Wang, R. Zhang, C. Wang, S. Xu and Y. Cui, *Biosens. Bioelectron.*, 2013, **41**, 745-751.
18 D. Li, H. Duan, Y. Ma and W. Deng, *Anal. Chem.*, 2018, **90**, 5719-5727.
19 S. Wang, K. Liu, X. Yao and L. Jiang, *Chem. Rev.*, 2015, **115**, 8230-8293.
20 X. Gao and L. Jiang, *Nature*, 2004, **432**, 36.
21 M. J. Liu, S. T. Wang and L. Jiang, *Nat. Rev. Mater.*, 2017, **2**, 17.
22 A. A. Popova, D. Marcato, R. Peravali, I. Wehl, U. Schepers and P. A. Levkin, *Adv. Funct. Mater.*, 2018, **28**, 1703486.
23 E. Ueda and P. A. Levkin, *Adv. Mater.*, 2013, **25**, 1234-1247.
24 A. N. Efremov, E. Stanganello, A. Welle, S. Scholpp and P. A. Levkin, *Biomaterials*, 2013, **34**, 1757-1763.
25 M. J. Hancock, F. Yanagawa, Y.-H. Jang, J. He, N. N. Kachouie, H. Kaji and A. Khademhosseini, *Small*, 2012, **8**, 393-403.
26 H. Yu, S. Peng, L. Lei, J. Zhang, T. L. Greaves and X. Zhang, *ACS Appl. Mater. Interfaces*, 2016, **8**, 22679-22687.
27 W. Feng, E. Ueda and P. A. Levkin, *Adv. Mater.*, 2018, DOI: 10.1002/adma.201706111, e1706111.
28 W. Shi, T. Xu, L. P. Xu, Y. Chen, Y. Wen, X. Zhang and S. Wang, *Nanoscale*, 2016, **8**, 18612-18615.
29 D. Tian, Y. Song and L. Jiang, *Chem. Soc. Rev.*, 2013, **42**, 5184-5209.
30 F. De Angelis, F. Gentile, F. Mecarini, G. Das, M. Moretti, P. Candeloro, M. L. Coluccio, G. Cojoc, A. Accardo, C. Liberale, R. P. Zaccaria, G. Perozziello, L. Tirinato, A. Toma, G. Cuda, R. Cingolani and E. Di Fabrizio, *Nat. Photon.*, 2011, **5**, 682-687.
31 H. Li, Q. Yang, J. Hou, Y. Li, M. Li and Y. Song, *Adv. Funct. Mater.*, 2018, DOI: 10.1002/adfm.201800448, 1800448.
32 Y. Lai, L. Lin, F. Pan, J. Huang, R. Song, Y. Huang, C. Lin, H. Fuchs and L. Chi, *Small*, 2013, **9**, 2945-2953.
33 Y. Song, T. Xu, L. P. Xu and X. Zhang, *Nanoscale*, 2018, **10**, 20990-20994.
34 H. Y. Zhao, J. Jin, W. J. Tian, R. Li, Z. Yu, W. Song, Q. Cong, B. Zhao and Y. Ozaki, *J. Mater. Chem. A*, 2015, **3**, 4330-4337.
35 Z. Wang, L. Feng, D. Xiao, N. Li, Y. Li, D. Cao, Z. Shi, Z. Cui and N. Lu, *Nanoscale*, 2017, **9**, 16749-16754.
36 S. Sun, D. Thompson, U. Schmidt, D. Graham and G. J. Leggett, *Chem. Commun.*, 2010, **46**, 5292-5294.
37 H. Zhang, T. Oellers, W. Feng, T. Abdulazim, E. N. Saw, A. Ludwig, P. A. Levkin and N. Plumere, *Anal. Chem.*, 2017, **89**, 5832-5839.
38 T. Xu, Y. Song, W. Gao, T. Wu, L. P. Xu, X. Zhang and S. Wang, *ACS Sens.*, 2018, **3**, 72-78.
39 L. P. Xu, Y. Chen, G. Yang, W. Shi, B. Dai, G. Li, Y. Cao, Y. Wen, X. Zhang and S. Wang, *Adv. Mater.*, 2015, **27**, 6878-6884.
40 T. Wu, T. Xu, Y. Chen, Y. Yang, L.-P. Xu, X. Zhang and S. Wang, *Sens. Actuator B Chem.*, 2018, **258**, 715-721.
41 Z. F. Gao, E. E. Sann, X. Lou, R. Liu, J. Dai, X. Zuo, F. Xia and L. Jiang, *NPG Asia Mater.*, 2018, DOI: 10.1038/s41427-018-0024-7.
42 T. Xu, W. Shi, J. Huang, Y. Song, F. Zhang, L. P. Xu, X. Zhang and S. Wang, *ACS Nano*, 2017, **11**, 621-626.
43 X. He, T. Xu, W. Gao, L. P. Xu, T. Pan and X. Zhang, *Anal. Chem.*, 2018, DOI: 10.1021/acs.analchem.8b04536.
44 S. S. Zhan, Y. Pan, Z. F. Gao, X. D. Lou and F. Xia, *Trends Anal. Chem.*, 2018, **108**, 183-194.
45 C. Wu, Q. Y. Cheng, S. Q. Sun and B. H. Han, *Carbon*, 2012, **50**, 1083-1089.
46 J. Rafiee, M. A. Rafiee, Z. Z. Yu and N. Koratkar, *Adv. Mater.*, 2010, **22**, 2151-2154.